International Journal of Nanomedicine

Dovepress
open access to scientific and medical research

Open Access Full Text Article

ORIGINAL RESEARCH

# AMP-Coated $TiO_2$ Doped ZnO Nanomaterials Enhanced Antimicrobial Activity and Efficacy in Otitis Media Treatment by Elevating Hydroxyl Radical Levels

Qianyu Bai[1,*], Yichi Zhang[1,*], Runqiu Cai[1], Haiyan Wu[1], Huiqun Fu[2], Xuemei Zhou[2], Jie Chai[3], Xuepeng Teng[3], Tianlong Liu[1]

[1]National Key Laboratory of Veterinary Public Health and Safety, College of Veterinary Medicine, China Agriculture University, Beijing, People's Republic of China; [2]101 Institute of the Ministry of Civil Affairs, Beijing, People's Republic of China; [3]Shandong Cancer Hospital and Institute, Shandong First Medical University and Shandong Academy of Medical Sciences, Jinan, People's Republic of China

*These authors contributed equally to this work

Correspondence: Xuemei Zhou, 101 Institute of the Ministry of Civil Affairs, South Fourth Ring West Road No.188, Beijing, 100070, Email zxmcaur@126.com; Tianlong Liu, College of Veterinary Medicine, China Agriculture University, Yuanmingyuan West Road No. 2, Beijing, 100193, Email liutianlong@cau.edu.cn



**Background:** In the past decades, antimicrobial resistance (AMR) has been a major threat to global public health. Long-term, chronic otitis media is becoming more challenging to treat, thus the novel antibiotic alternative agents are much needed.

**Methods:** ZnO@$TiO_2$@AMP (ATZ NPs) were synthesized through a solvothermal method and subjected to comprehensive characterization. The in vitro and in vivo antibacterial effect and biocompatibility of ATZ NPs were evaluated. For the antibacterial mechanism exploration, we utilized the Electron Paramagnetic Resonance (EPR) Spectrometer to detect and analyze the hydroxyl radicals produced by ATZ NPs.

**Results:** ATZ NPs exhibited a spherical structure of 99.85 nm, the drug-loading rate for ZnO was 20.73%, and AMP within ATZ NPs was 41.86%. Notably, the Minimum Inhibitory Concentration (MIC) value of ATZ NPs against *Staphylococcus aureus* (*S. aureus*), methicillin-resistant *Staphylococcus aureus* (MRSA), and *Streptococcus pneumoniae* (*S. pneumoniae*) were 10 μg/mL, and Minimum Bactericidal Concentration (MBC) value of ATZ NPs against *S. aureus*, and *S. pneumoniae* were 50 μg/mL. In comparison to the model group, the treatment of otitis media with ATZ NPs significantly reduces inflammatory exudation in the middle ear cavity, with no observable damage to the tympanic membrane. Both in vivo and in vitro toxicity tests indicating the good biocompatibility of ATZ NPs. Moreover, EPR spectroscopy results highlighted the superior ability of ATZ NPs to generate hydroxyl radicals (·OH) compared to ZnO NPs.

**Conclusion:** ATZ NPs exhibited remarkable antibacterial properties both in vivo and in vitro. This innovative application of advanced ATZ NPs, bringing great promise for the treatment of otitis media.

**Keywords:** nanoparticles, otitis media, zinc oxide, mesoporous titanium dioxide, antimicrobial peptide, antimicrobial, hydroxyl radical

## Introduction

In the past decades, antimicrobial resistance (AMR) has been a major threat to global public health.[1,2] With the increasing emergence of multi-drug resistant (MDR) bacteria, we have entered the post-antibiotic era, there is an urgent demand for the discovery and development of novel, highly effective antibiotic candidates.[3–5] Inflammation in the ear, particularly otitis media, poses considerable treatment challenges due to the ear canal's unique anatomy, hindering direct

Received: 14 November 2023
Accepted: 6 March 2024
Published: 26 March 2024

access for therapeutic drugs. As AMR problem worsens, there is a lack of ideal medications for otitis media treatment, and severe cases may result in hearing impairment.[6–9]

To tackle this, researchers have been striving to develop novel antibiotic alternatives, such as zinc oxide nanoparticles (ZnO NPs), titanium dioxide nanoparticles ($TiO_2$ NPs), and antimicrobial peptides (AMPs). Each of these drugs has its own strengths in antibacterial properties, yet they also come with their own limitations. ZnO NPs, typically around 10 nm in size, exhibit notable antimicrobial properties by generating reactive oxygen species (ROS) on bacterial membranes, presenting a promising agent for combating such infections.[10–12] However, these tiny ZnO NPs exhibit poor selectivity to cells and significant cytotoxicity.[13,14] Mesoporous core-shell $TiO_2$ NPs have specific surface area, narrow pore size distribution, photochemical stability, and the capacity for surface properties modification.[15–18] $TiO_2$ NPs can also produce ROS under ultraviolet (UV) photocatalysis. However, its antibacterial properties are limited due to the dependence of UV light. Studies have shown that by doping with ZnO NPs, the light absorption range of $TiO_2$ nanoparticles can be shifted to visible light, providing a solution to overcome the shortcomings of $TiO_2$ in applications.[19–23] Inorganic materials such as ZnO and $TiO_2$ also have limitations such as low selectivity and cytotoxicity, requiring the strategies to enhance their cell selectivity to broaden their application range.[24,25] Antimicrobial peptides (AMPs) are promising antibiotic alternative candidate with excellent selectivity. They possess a positive surface charge, typically ranging from +2 mv to +11 mv. By binding to negatively charged molecules on bacterial membranes, AMPs selectively adsorb to bacteria, then insert hydrophobic groups into the phospholipid bilayer, ultimately leading to membrane disruption and cytoplasm leakage, thereby killing bacteria.[26–29]

Herein, novel composite nanoparticles ZnO@$TiO_2$@AMP (ATZ NPs) are reported as a potent antibiotic agent for treating otitis media for the first time. During the synthesis of zinc oxide, $TiO_2$ NPs were incorporated to mitigate the toxicity of ZnO NPs, and AMPs were introduced to enhance the material's biocompatibility. Our results show that ATZ NPs exhibited synergistic antibacterial effects in vitro compared to the individual application of AMPs and ZnO NPs. Moreover, the nanoparticles exhibited remarkable efficacy in combating otitis media in mice, effectively reducing the inflammatory response. This study also revealed that ATZ NPs inflicted more severe membrane damage in bacteria by generating higher levels of hydroxyl radicals (·OH). Overall, this work provides a promising antibiotic alternative candidate, bridging the gap in clinical treatment drugs for otitis media.

# Materials and Methods

## Materials

Zinc acetate dihydrate ($Zn(Ac)_2 \cdot 2H_2O$ (LA:GA=50:50)) was purchased from Daigang Biological Engineering Co., LTD. (Jinan, China); Methyl Sulfonyl Methane (MSM) was purchased from Sinopharm Group Chemical Reagent Company; Methanol and KOH were purchased from Guangda Hengyi (Beijing, China); Mesoporous $TiO_2$ NPs were purchased from Yanqui Information Technology (Hangzhou, China); AMP (CATH-1) was purchased from Liuhe huada Gene Technology Co., LTD. (Beijing, China). The above chemical reagents belong to analytic-reagent grade. The *S. aureus* ATCC6538, MRSA ATCC 33591, and *S. pneumoniae* NCTC 7466 isolates were generously provided by the College of Veterinary, China Agricultural University.

## Synthesis and Characterization of Nanoparticles ZnO@$TiO_2$@AMP (ATZ NPs)

A modified "solvothermal method" was employed to synthesize TZ NPs followed by the addition of AMP through oscillatory absorption.[30,31] In brief, solution A: solution containing 2.25g $TiO_2$ was centrifugated at 8000rpm for 5 minutes and washed with methanol 3 times. The obtained precipitate was dispersed in 75mL methanol. Solution B: 2.75g $Zn(Ac)_2 \cdot 2H_2O$ and 1g dimethyl sulfone (DMSO) were dissolved in 75mL methanol. Solution A and B were mixed on a magnetic mixer, 200rpm (IKA, Germany). The temperature rapidly rose to 60°C, then slowly increased to 65°C, at this temperature for 1 hour. Solution C: 1.47g KOH, ultrasonically dispersed in 25mL methanol, was then added to solution AB at the rate of 1 drop /2s. The reaction was allowed to proceed for 2.5 hours. Subsequently, TZ NPs was centrifuged at 6000rpm, 5 minutes, followed by washing the precipitate with methanol three times and then with distilled water three times. AMP solution was then added, under the influence of electrostatic force, ATZ NPs were produced.

The size and morphology characterization of ZnO NPs, TZ NPs and ATZ NPs were determined using Transmission electron microscopy (JEM-F200, JEOL, Japan). The Energy Disperse Spectroscopy (EDS, JEM-F200, JEOL, Japan) and

high-resolution TEM (TEM, HT7700, Hitachi, Japan) were employed for analyze the bulk distribution of Zn, Ti, N, and O in ATZ NPs. Moreover, the drug-loading rate of ZnO and AMP in ATZ NPs was measured by Inductively Coupled Plasma-Mass Spectrometry (ICP-MS) and the BCA method, respectively. The hydrated particle size of ATZ NPs was determined through Dynamic Light Scattering (DLS) methods, and the zeta potential of ATZ NPs was measured by a Zetasizer (ZS90, Malvern Zetasizer, UK).

## Antibacterial Effect of ATZ NPs in vitro

The determination of Minimum Inhibitory Concentration (MIC) and Minimum Bactericidal Concentration (MBC) were based on the method of Clinical and Laboratory Standards Institute (CLSI).[32] This method employed microdilution to determine the MIC of various materials against *S. aureus*, MRSA, and *S. pneumoniae*, each material was tested in two parallel groups. The materials were serially diluted to final concentration of 500, 200, 100, 10, 1μg/mL, respectively. Subsequently, 100μL of each dilution was added to a 96-well plate pre-inoculated with 100μL of bacterial solution. The control group comprised the following, Control Check (CK): containing only sterile Luria-Bertani (LB) medium, negative control: containing 100μL bacterial suspension and 100μL LB medium, positive control: 90μL bacteria suspension, 10ul antibiotics and 100μL LB medium. The final concentration of bacterial suspension in different wells was adjusted to 1×10^5CFU/mL. The 96-well plates were incubated at 37°C in an incubator for 18 hours, followed by the addition of 20 μL of 0.0625% resazurin solution to each well. Incubation continued for an additional 4 hours, and the inhibition effect was assessed based on observed color changes.

MBC is the minimal drug concentration of the drug to eradicate 99.9% of the microorganism (equivalent to 3 orders of magnitude). To further assess the antibacterial property of ATZ NPs, the MBC of different materials against *S. aureus* and *S. pneumoniae* were tested. Following a procedure similar to the MIC test, 100μL of different concentrations of materials (500, 200, 100, 50μg/mL) were added to a 96-well plate and co-cultivated with 100μL of bacteria at 37°C for 2 hours. Liquid from the wells without visible sediment was then inoculated onto Petri dishes at 37°C for 24h, after which the colony count was measured. Each test was repeated three times.

To investigate the interactions between ATZ NPs and bacteria cells, the integrity of cell membranes was examined using the scanning electron microscopy (SEM, ZEISS Gemini 300, Germany). Bacterial suspensions were incubated with different materials at a concentration of 200 μg/mL at 37°C for 2 hours, while a control group consisted of bacteria mixed with a PBS solution. Then the mixed liquid was centrifuged for 20 minutes, underwent three cycles of washing and resuspension, and the bacteria were fixed with 2.5% glutaraldehyde and followed by a series of procedures according to Cao's method.

## Antibacterial Effect of ATZ NPs in vivo

In this study, mice were raised in accordance with the guidelines established by the Experimental Animals Authority of Beijing and received approval from the Animal Ethics Committee of China Agricultural University. Mice in the model groups were inoculated with a suspension of *S. pneumoniae* suspension (5μL per mouse, 1×10^8 CFU $mL^{-1}$) in the tympanic cavity. The healthy control group received no injections, while the PBS group was administered with PBS only. On the first day after infection, a suspension of ZnO NPs, AMP and ATZ NPs (5uL 50μg $mL^{-1}$ materials per mouse, respectively) were taken with a micro sampler and dropwise added into the bilateral ear canals of corresponding group of model mice and repeated on the second day. Mice were weighed daily. On the 3rd day after treatment, they were euthanized. Bilateral middle ear tissue was harvested following ear resection and fixed in a 10% formaldehyde solution. Subsequently, the tissue was stained by hematoxylin and eosin (H.E.), and the histological morphology of the middle ear cavity in mice was observed under microscope (Nikon, Y-TV55, Japan) and TEM (HT7700, Hitachi, Japan). Additionally, blood routine examinations were evaluated by the laboratory at the College of Veterinary Medicine, China Agricultural University.

## Evaluation of Biocompatibility

A hemolysis test was conducted to assess the biocompatibility of ATZ NPs, red blood cells (RBC) of New Zealand rabbit were employed. Precipitated RBCs were collected and resuspended in PBS to get 2% RBC suspension (v/v). PBS group served as the negative control, while RBC treated with 1% TritonX-100 served as the positive control. The nanoparticles were diluted to various concentrations (50, 100, 150, 200 and 250μg $mL^{-1}$, respectively), with three parallel sets in each

group. Additionally, incubated with the different nanoparticles at 37°C for 1 hour. The samples were then centrifuged at 4°C, 1500rpm for 15 minutes, and 100 μL of the supernatant was transferred to a 96 wells plate. A microplate reader (BioRad, iMark, USA) was utilized to calculate the relative hemolysis rate.

To evaluate the potential toxicity of ATZ NPs administered through the ear canal, 30 ICR mice (6-week-old males, weighing 20g) were randomly divided into 5 groups: a Control (untreated) group, a ZnO NPs group and an AMP group (both at a concentration of 500μg mL-1, respectively), 200 μg $mL^{-1}$ ATZ NPs ($ATZ_{200}$) group and 500μg $mL^{-1}$ ATZ NPs ($ATZ_{500}$) group. After administrated through the external ear canal, the mice were weighed every two days. On the 7th day, the mice were sacrificed, and their blood parameters were analyzed, along with the histopathological examination of major organs using H&E.

## Electron Paramagnetic Resonance Spectrometer (EPR) Measurements

ZnO NPs and ATZ NPs were dispersed in aqueous solutions for the measurement of hydroxyl radicals. Dimethyl Pyrroline Oxide (DMPO, Sigma-Aldrich Co) served as the trapping agent was. Suspension of ZnO NPs and ATZ NPs were incubated with DMPO and exposed to UV irradiation for 5 minutes. The samples were loaded into capillary tubes and analyzed using an electron paramagnetic resonance spectrometer (Bruker EMX nano, Germany) to quantify the intensity of hydroxyl radical generated by the nanomaterials.

## Statistical Analysis

The experimental data were represented as the mean ± SD. Differences between groups were analyzed using a one-way analysis of variance (ANOVA) conducted with GraphPad Prism 8.0 (CA, USA), and significance was determined at $p<0.05$.

# Results

## Synthesis and Characterization of Nanoparticles ZnO@$TiO_2$@AMP (ATZ NPs)

In the present study, ATZ NPs were successfully synthesized by a modified "solvothermal method" followed by the addition of AMP via oscillatory absorption (Figure 1A). TEM images revealed that individual ZnO nanoparticle had a crystalline structure with an average particle size of 8.75nm. Each TZ NP displayed a spherical structure measuring 98.95 nm, featuring a hollow interior and a rough surface adored with numerous of ZnO NPs. ATZ nanoparticles exhibited a spherical morphology of 99.85 nm, with ZnO NPs still observable on the surface. However, the surface appeared smoother due to the presence of the AMP coating (Figure 1B). The Energy Dispersive Spectroscopy (EDS) mapping results manifested that ATZ NPs contained element O, Ti, N and Zn (Figure 1C). The drug-loading rate of ZnO determined to be 20.73% using inductively coupled plasma-mass spectrometry (ICP-MS), while that of AMP in ATZ NPs was 41.86%, as measured by the BCA method (Figure 1D). The hydrated particle size of ATZ NPs was determined by dynamic light scattering (DLS) (Figure 1E). The hydrated particle size of ATZ NPs ranged from 121.65nm to 293.82nm, with an average particle size of 204.96nm. Moreover, the zeta potential of ATZ NPs was shown in Figure S1. Upon the addition of AMP, the potential of the nanoparticles shifted from −10.17mV to +33.04mV, which can be attributed to the positively charged surface of AMP. This result also confirmed the successful adsorption of AMP.

## Antibacterial Effect of ATZ NPs in vitro

In this section, the antimicrobial properties of ATZ NPs were assessed against *S.aureus*, MRSA, and *S.pneumoniae*,[33,34] The MIC of different materials were shown in Figure 2A, the resazurin indicator changes color from blue to pink upon interaction with bacteria. In this context, blue wells indicated negative results, signifying no bacterial growth, while pink wells indicated positive results, with the first well turning blue representing the MIC of the material. The MIC of ZnO NPs against *S. aureus*, MRSA and *S. pneumoniae*, was found to be 50 μg $mL^{-1}$. Meanwhile, the MIC of AMP against *S. aureus*, MRSA and *S. pneumoniae*, was 10 μg $mL^{-1}$, 50 μg mL-1, and 10 μg $mL^{-1}$, respectively. The MIC values of ATZ NPs against these bacterial strains were all 10 μg $mL^{-1}$ (Figure 2A). Considering the lower actual ZnO and AMP contents in ATZ, the above results indicated the superior inhibitory properties of ATZ NPs against *S. aureus*, MRSA, and *S. pneumoniae*.

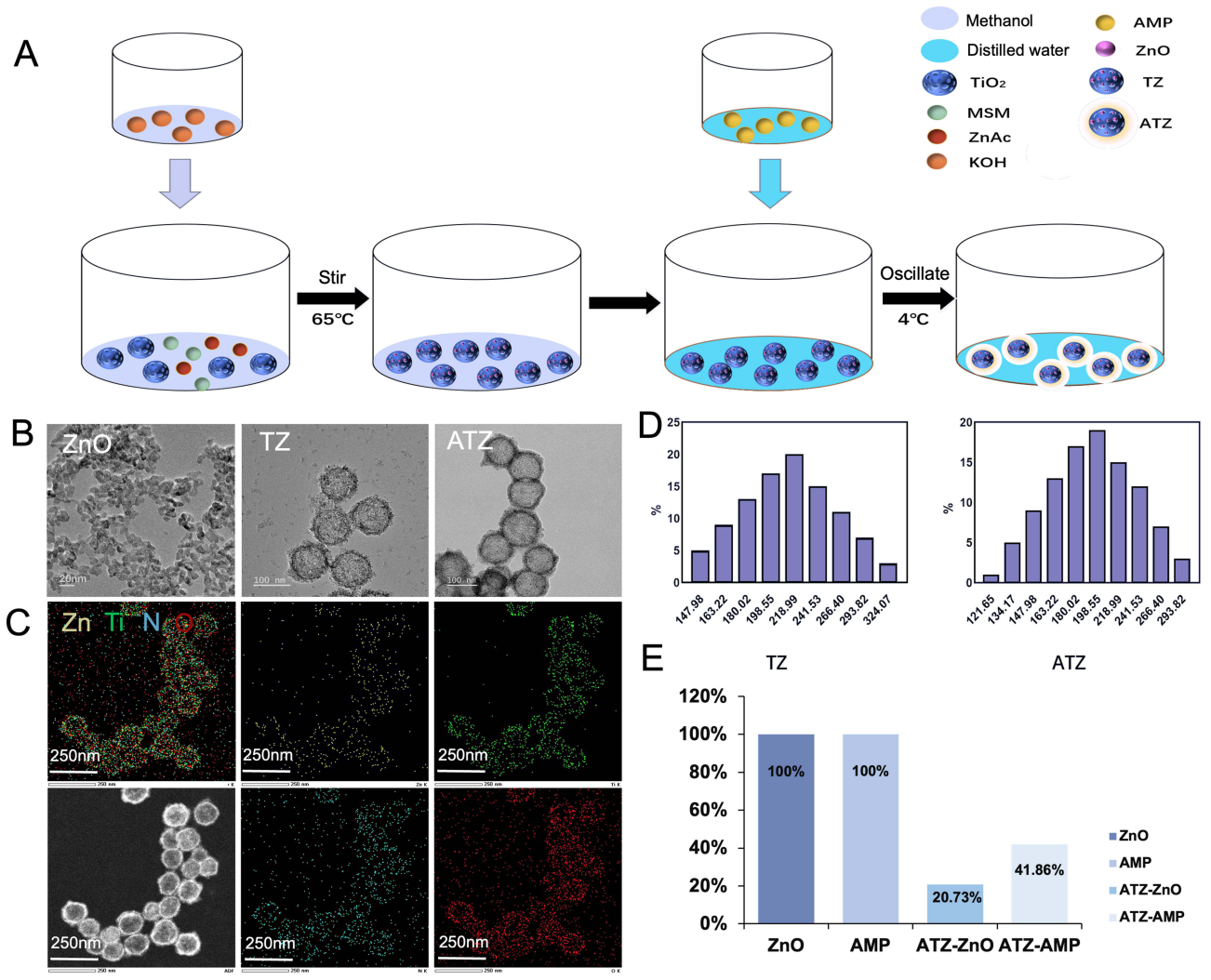


**Figure 1** Synthesis and characterization of ATZ NPs. (**A**) Scheme for preparation of ATZ nanoparticles. (**B**) TEM images of ZnO NPs, TZ NPs and ATZ NPs. (**C**) The EDS mapping images of ATZ NPs. (**D**) Content proportion of ZnO and AMP components in ATZ NPs. ZnO NPs, AMP and ATZ NPs were at the same concentration. (**E**) Hydrated particle size of TZ NPs and ATZ NPs determined by DLS method.

The MBC of various materials against *S. aureus* and *S. pneumoniae* were depicted in Figure 2B. The colony counts of *S. aureus* and *S. pneumoniae* co-cultivated with 50 μg $mL^{-1}$ ATZ NPs exhibited a reduction by three orders of magnitude. In contrast, the antimicrobial effects of ZnO NPs and AMP at the same concentration were less pronounced. These findings further underscore the superior antibacterial efficacy of ATZ NPs when compared to ZnO NPs and AMP.

Figure 2C showed scanning electron microscopy (SEM) images of *S. pneumoniae* and *S. aureus* interacted with different materials over a 2-hour period. In comparison to the control group, the morphology of *S. pneumoniae and S. aureus* treated with ATZ NPs exhibited severe alterations, including evident membrane damage and cytoplasm leakage. These changes indicated that ATZ NPs have significantly damaged the cytomembrane. Conversely, treatment with ZnO NPs or AMP resulted in milder damage to S. pneumoniae and S. aureus when compared to ATZ NPs. It is important to note that the content of ZnO and AMP in ATZ NPs was only 20.73% and 41.86% of that found in ZnO NPs and AMP at the same concentration, respectively. This enhancement in antibacterial efficacy in ATZ NPs suggests a synergistic effect resulting from the combination of ZnO NPs, mesoporous $TiO_2$ NPs and AMP.

## Antibacterial Effect of ATZ NPs in vivo

The local administration of ATZ NPs in mice was assessed for its antibacterial and healing effects, as illustrated in Figure 3A. On the third day after treatment, the cure rate of ATZ NPs group reached 83.33%. Histopathological

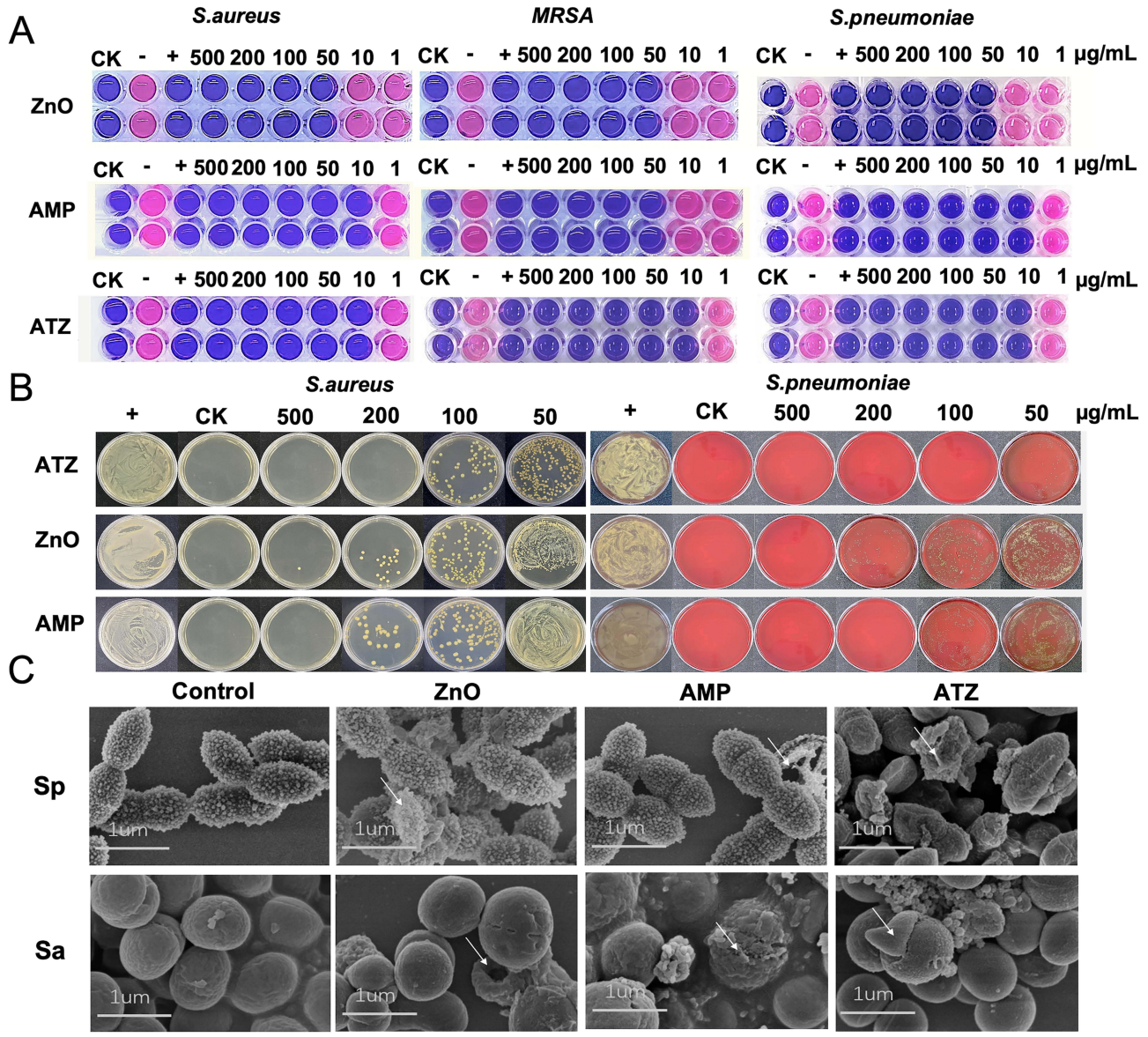


**Figure 2** Antibacterial effect of different materials in vitro. (**A**) MIC against *S. aureus*, MRSA and *S. pneumoniae* isolates. CK: control check; "-": negative control; "+": positive control. (**B**) MBC against *S. aureus* and *S. pneumoniae* isolates. (**C**) SEM images of *S.pneumoniae* (Sp) and *S.aureus* (Sa) after co-cultivated with ZnO NPs, AMP and ATZ NPs.

examination revealed that the model group represented a severe inflammatory response, characterized by significant inflammatory hyperplasia in the tympanic tissue and a substantial amount of exudation in the middle ear cavity. In contrast, mice treated with ZnO NPs, AMP, and ATZ NPs manifested reduced inflammatory exudate in the middle ear cavity with no significant lesions observed in the middle ear. These findings indicating that ATZ NPs have pleasant antibacterial efficacy and healing property (Figure 3B).

To inspect the ultrastructure of middle ear, we employed TEM to assess the morphology change of the middle ear. TEM images revealed the tympanic striated muscles of mice in healthy group were neatly arranged. However, in the untreated model group, rhabdomyolysis and damage to the tissue structure damage were observed. Notably, the tissue morphology of the ATZ NPs-treated group had recovered to a state similar to that of the control group, with no significant histopathological lesion was observed (Figure 3C).

There were no significant differences in body weight and blood routine examination results between the NPs treatment groups and the control group (Figure 3D). In contrast, the average body weight of mice in the model group was significantly decreased, and the level of white blood cells (WBC) significantly increased, indicating the local

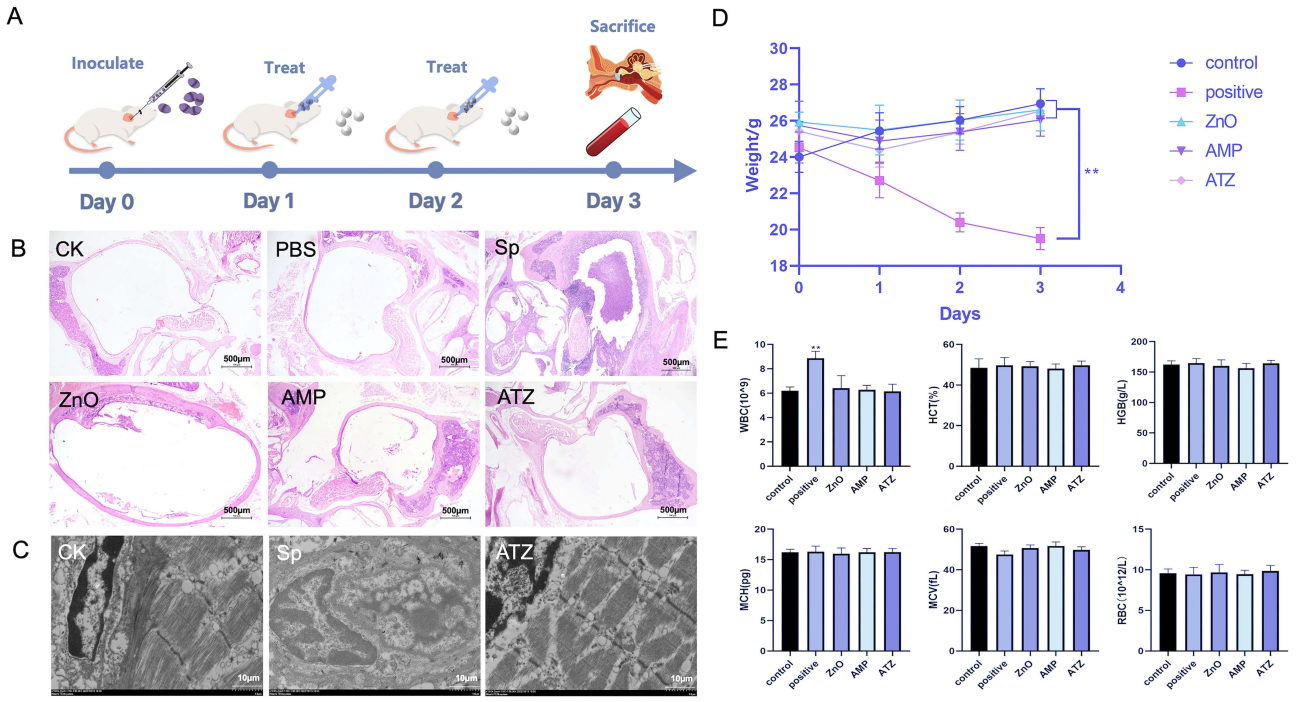


**Figure 3** Antibacterial effect of different nanomaterials in vivo. (**A**) Scheme of ICR mice otitis media treatment. (**B**) Histopathological assessment in different groups of ICR mice. CK: control check. Scale bar = 500 μm. (**C**) Ultra-pathological assessment of the middle ear cavity. Scale bar = 10 μm. (**D**) Weight change of ICR mice during the treatment. (**E**) The blood routine examination of ICR mice. Data was represented as mean ± SD (**p < 0.01, n ≥ 3).

administration of ATZ NPs could effectively regulate the inflammatory response back to normal levels, hence improving the therapeutic properties for otitis media (Figure 3E).

## Biocompatibility of ATZ NPs

The biocompatibility of ATZ NPs was probed for the eligibility for further application. Initially, RBCs were co-cultivation with different concentrations of materials. The negative group was treated with PBS, and the positive control group was treated with TritonX-100. When combining the results from both positive and negative groups, no obvious hemolysis was observed in NPs treated groups (Figure 4A). Further, relative hemolysis rate was calculated based on the optical density (OD) of the supernatant in each group. The hemolysis rate of ATZ NPs at a concentration of 250 μg $mL^{-1}$ measured at 4.7% (Figure 4B). Compared to this, the hemolysis rate of RBC treated with AMP, ZnO NPs and $TiO_2$ NPs were determined to be 5.3%, 9.55% and 7.73%, respectively. These rates were significantly higher than that of the ATZ NPs group ($p<0.05$), indicating the favorable biocompatibility of ATZ NPs.

For the in vivo toxicity test, drugs were administered locally through the mice's ear canal. The weight of mice was measured daily after administration and there were no significant differences among all groups (Figure 4C). Simultaneously, the results of blood routine examinations in various groups remained within the normal range (Figure 4D). H&E staining demonstrated that there were no significant histopathological changes in major organs, including heart, liver, spleen, lung, and kidney. As depicted in Figure 5, the histopathological changes in major organs were assessed in the AMP group, ZnO NPs group, 200 μg $mL^{-1}$ ATZ NPs ($ATZ_{200}$ NPs) group, and 500 μg $mL^{-1}$ ATZ NPs ($ATZ_{500}$ NPs) group. The results showed that, in the heart, myocardial fibers were neatly arranged without degeneration. Similarly, hepatic cords in the liver were orderly without any evidence of necrosis. Moreover, there was no noticeable exudate in the glomeruli, and the tubular epithelium appeared intact, suggesting no histopathological alterations in the kidneys. In the spleen, both the red pulp and white pulp were distinctly demarcated, with visible lymphoid follicles. Furthermore, there were no indications of fibrosis or exudate in the pulmonary alveoli, nor any infiltration of inflammatory cells around the pulmonary blood vessels, indicating no lung damage. All these results collectively suggest that ATZ NPs exhibit good biocompatibility both in vitro and in vivo.

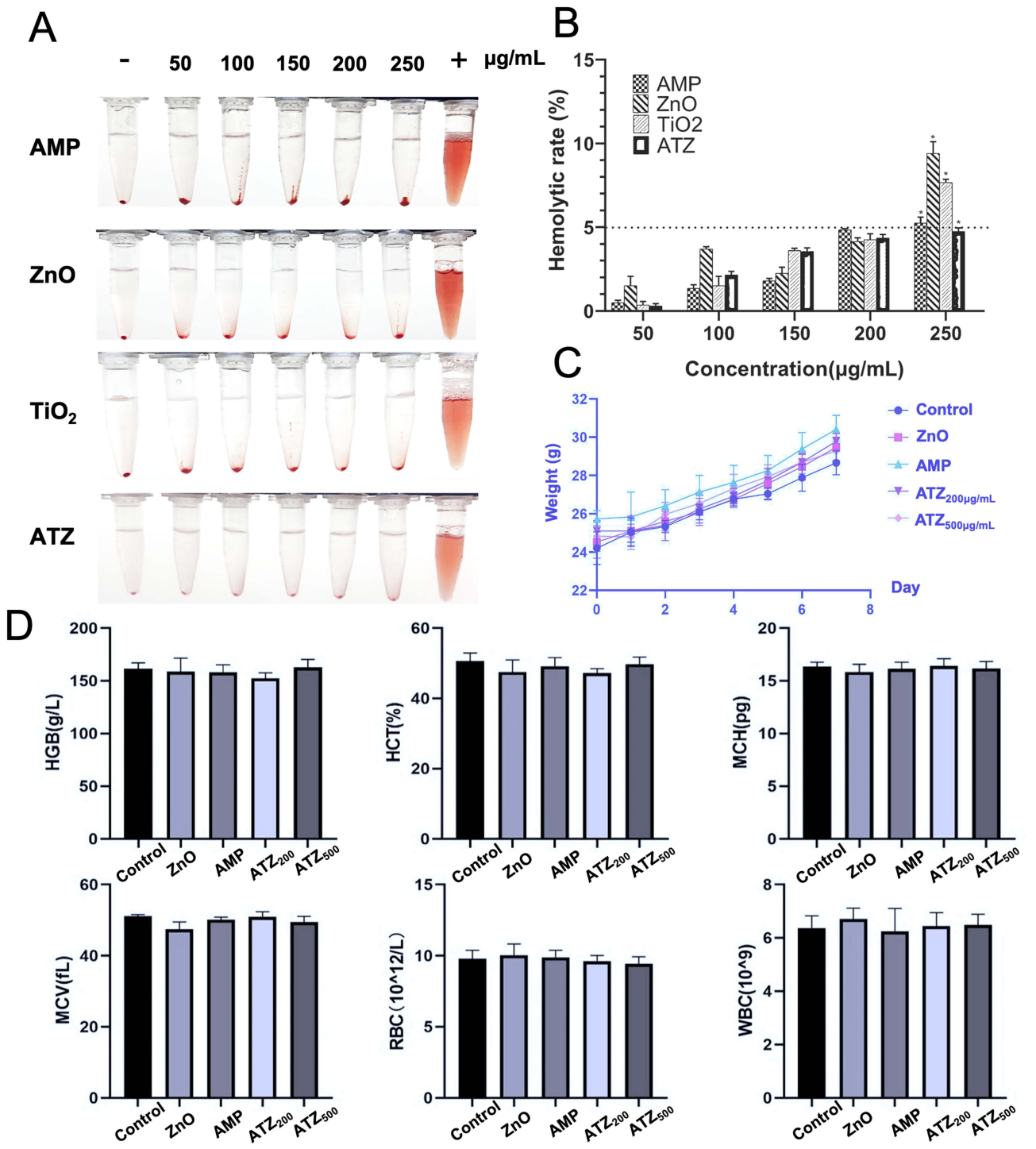


**Figure 4** Biocompatibility evaluation of ATZ NPs in vitro and in vivo. (**A**) Hemolysis test of AMP, ZnO, $TiO_2$ and ATZ NPs (**B**). Relative hemolysis rate of ZnO, $TiO_2$, AMP and ATZ NPs (n=3). (**C**) Weight change of ICR mice in toxicity test. (**D**) Blood routine examination of mice in toxicity tests. $ATZ_{200}$ and $ATZ_{500}$ refer to the treatment group with 200 μg $mL^{-1}$ and 500μg $mL^{-1}$ ATZ NPs, respectively. Data was represented as mean ± SD (*p < 0.05, n ≥ 3).

## Electron Paramagnetic Resonance (EPR) Spectroscopic Analysis

One of the primary mechanisms through which nanomaterials such as ZnO NPs inhibit microorganisms is by generating an abundance of ROS. To investigate whether ATZ NPs combat bacterial by inducing a high-level ROS burst, we employed the EPR spectroscopy to measure the radicals produced by ATZ NPs compared with small nanosized ZnO, which has been proved to kill germ by highly efficient generation of ROS.

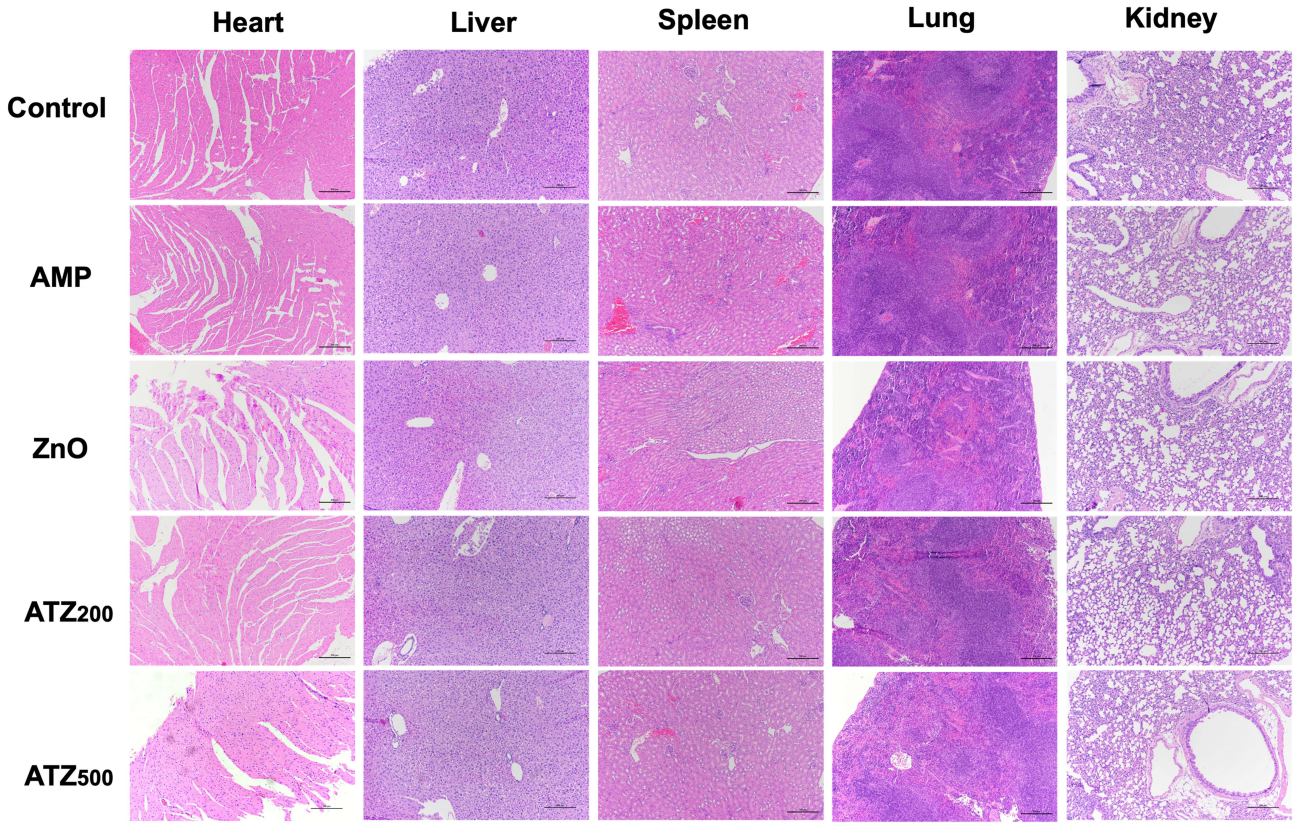


**Figure 5** Histopathological section of ICR mice. H.E staining of major organs (heart, liver, spleen, lung and kidney) at 7 days after locally administrated with materials, no obvious histological lesion was observed. $ATZ_{200}$ and $ATZ_{500}$ refer to the treatment group with 200 μg $mL^{-1}$ and 500μg $mL^{-1}$ ATZ NPs, respectively. Scale bar = 200 μm.

As shown in Figure 6A, after 5 minutes of UV irradiation, both ZnO NPs and ATZ NPs samples exhibited similar EPR spectra. The characteristic 1:2:2:1 quartet EPR spectrum of hydroxyl radicals (·OH) were observed (Figure 6B). Compared with ZnO NPs, ATZ NPs represented increasing peak signals, while in the absence of UV irradiation, no signal

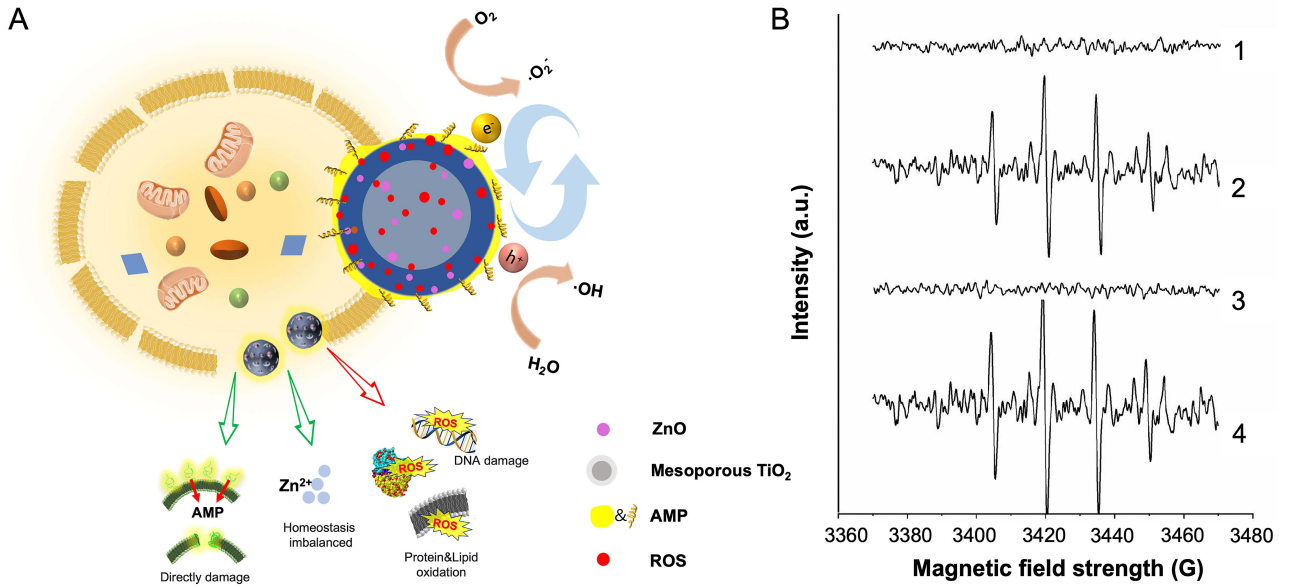


**Figure 6** Antibacterial mechanism investigate of ATZ NPs. (**A**) Illustration of the antibacterial mechanism of ATZ NPs. (**B**) EPR spectra of hydroxyl radicals generated by ZnO NPs and ATZ NPs: 1 and 3 refer to ZnO NPs and ATZ NPs before UV irradiation; 2 and 4 refer to ZnO NPs and ATZ NPs after UV light irradiation.

was observed. It should be noted that, at the same concentration, the actual content of ZnO in ATZ NPs (20.73%) was much less than that in ZnO NPs (100%). The increase in peak intensities indicated that hydroxyl radicals generated from ATZ NPs were more abundant than those generated from free ZnO.

## Discussion

Due to the developing severe antimicrobial resistance (AMR) problem and anatomical limitations of ear canal, refractory otitis media lacks effective clinical treatments. Prolonged infections can ultimately result in hearing loss.[35,36] There's an urgent need for highly effective antimicrobial agents that are less prone to inducing bacterial antibiotic resistance as alternatives to address this treatment challenge. Zinc-based nanomaterials have shown great potential in the field of antimicrobials due to their unique physical and chemical properties, coupled with a multi-mechanism synergistic antibacterial strategy. However, existing research of zinc-based nanomaterials exhibit certain limitations, including inadequate bacterial selectivity, elevated toxicity, and an unclear understanding of the antibacterial mechanisms.[37,38]

To tackle the challenges mentioned above, this paper introduces a novel nanomaterial termed ZnO@$TiO_2$@AMP (ATZ NPs), synthesized via solvothermal method, where ZnO NPs was doped onto $TiO_2$ NPs and AMP is adsorbed through oscillatory adsorption. Antibacterial effects in vitro indicated that ATZ NPs possess significant higher antibacterial activity compared to ZnO NPs and AMP alone, with about 12 times and 25 times greater inhibition activity against MRSA at the same concentration, respectively. Subsequently, we assessed the eligibility of clinical application of ATZ NPs on *S. pneumoniae* infected otitis media in mice. H&E staining and ultrastructure images revealed that the tissue morphology of the ATZ NPs-treated group had fully recovered to match that of the healthy group, that local administration of ATZ NPs had a good therapeutic effect on otitis media and could ameliorate the inflammation-induced damage.

In exploring the antimicrobial mechanisms, EPR spectroscopy showed that ATZ NPs generated higher level of hydroxyl radicals compared to ZnO NPs. One possible explanation for this phenomenon is that ATZ NPs have lower charge transfer resistance or higher conductivity than free ZnO NPs, enabled ZnO current carriers to exhibit greater transfer efficiency, resulting in the production of a higher level of hydroxyl radicals (·OH). This finding aligns with the research conducted by Smijs and Bishweshwar, who elaborated that under UV irradiation, photogenerated holes enter the valence band of ZnO from the valence band of $TiO_2$. These holes react with $H_2O$ to form ·OH, known as one of the most powerful oxidizing agents.[39–42] Mesoporous $TiO_2$, owing to its large specific surface area, facilitates the concentration of free radicals on its surface, resulting in the ROS outbreak.[43–45] The concentrated ZnO NPs may perform dual bactericidal functions. Together with the generation of ROS, large amount of $Zn^{2+}$ were released during the interaction with germs. The excess $Zn^{2+}$ concentration disrupts bacterial cell ion channels, leading to intracellular environment disturbance and cytoplasmic leakage.[46–50] Simultaneously, AMP in ATZ NPs could cleave bacteria by inserting the hydrophobic amino acids residue into the bacterial membranes then destroying bacterial cell membranes, performing synergistic antibacterial property. Different from the antibiotics, ATZ NPs interact with and penetrate bacterial membrane through a physical strategy. Generating mutations to resist membrane damage is costly because it may reduce the viability of bacteria seriously, and the rate at which bacteria produce enzymes that degrade ATZ NPs cannot compete with the rapid bactericidal effect of ATZ NPs, consequently, it is difficult for bacteria to develop resistance.[51–55]

The physicochemical properties of nanomaterials play a pivotal role in shaping their biological characteristics.[56,57] Smaller nanoparticles exhibit higher antibacterial activity but increased cytotoxicity.[58] In our study, we combined ZnO NPs with hollow mesoporous $TiO_2$, maintaining the individual size of ZnO NP while increasing the overall volume to 98.95 nm. No signs of hematolysis were observed after the incubation with ATZ NPs. The body weight of mice and the results of the blood routine examinations were within the normal range, histological evaluation results showed that ATZ NPs did not cause any toxicity to major organs. Collectively, these biocompatibility test results affirmed the good biocompatibility of ATZ NPs. Thus, it presents excellent biocompatibility both in vivo and in vitro.

## Conclusion

In summary, this study successfully synthesized ATZ NPs. In terms of antimicrobial mechanisms, the introduction of $TiO_2$ NPs expanded the antibacterial capacity of ZnO NPs, inducing a higher-level generation of ·OH compared to ZnO NPs and the cytotoxicity caused by excessively small particle size was reduced. Furthermore, the introduction of AMP

enhanced the material's selectivity. The present work has verified that ATZ NPs manifested pleasant antibacterial activity against clinical drug-resistant strains and provide favorable therapeutic effects in the treatment of otitis media in mice.

Overall, the utilization of hollow mesoporous $TiO_2$ NPs to carry antibacterial active agents such as ZnO NPs represent an innovative strategy for the development of novel antibiotic candidates, with great application potential in the clinical settings to address otitis media.

## Acknowledgments

The authors acknowledge the financial support from the National Key R&D Program of China, Grant/Award Number: 2022YFC3800405.

## Disclosure

The authors report no conflicts of interest in this work.

## References

1. Helmy YA, Taha-Abdelaziz K, Hawwas HAEH, et al. Antimicrobial Resistance and Recent Alternatives to Antibiotics for the Control of Bacterial Pathogens with an Emphasis on Foodborne Pathogens. *Antibiotics*. 2023;12(2):274. doi:10.3390/antibiotics12020274
2. Rizzo A, Piccinno M, Lillo E, Carbonari A, Jirillo F, Sciorsci RL. Antimicrobial Resistance and Current Alternatives in Veterinary Practice: a Review. *Curr Pharm Des*. 2003;29(5):312–322.
3. Shen Z, Guo Z, Zhou L, et al. Biomembrane induced in situ self-assembly of peptide with enhanced antimicrobial activity. *Biomater Sci*. 2020;8 (7):2031–2039. doi:10.1039/C9BM01785B
4. Ghosh S, Mukherjee R, Mukherjee S, Barman S, Haldar J. Engineering Antimicrobial Polymer Nanocomposites: *in Situ* Synthesis, Disruption of Polymicrobial Biofilms, and *In Vivo* Activity. *ACS Appl Mater Interfaces*. 2022;14(30):34527–34537. doi:10.1021/acsami.2c11466
5. Naheed S, Din IU, Qamar MU, et al. Synthesis, Anti-Bacterial and Molecular Docking Studies of Arylated Butyl 2-Bromoisonicotinate Against Clinical Isolates of ESBL-Producing Escherichia coli ST405 and Methicillin-Resistant Staphylococcus aureus. *IDR*. 2023;16:5295–5308. doi:10.2147/IDR.S407891
6. Tambs K, Hoffman HJ, Borchgrevink HM, Holmen J, Samuelsen SO. Hearing loss induced by noise, ear infections, and head injuries: results from the Nord-Trøndelag Hearing Loss Study: hipoacusia inducida por ruido, infecciones de oído y lesiones cefálicas: resultados del estudio Nord-Trøndelag sobre pérdidas auditivas. *Int J Audiol*. 2003;42(2):89–105. doi:10.3109/14992020309078340
7. Monroy GL, Pande P, Shelton RL, et al. Non-invasive optical assessment of viscosity of middle ear effusions in otitis media. *J Biophotonics*. 2017;10(3):394–403. doi:10.1002/jbio.201500313
8. Dettori S, Portunato F, Vena A, Giacobbe DR, Bassetti M. Severe infections caused by difficult-to-treat Gram-negative bacteria. *Current Opinion in Critical Care*. 2023;29(5):438. doi:10.1097/MCC.0000000000001074
9. Prasad A, Hasan SMA, Gartia MR. Optical Identification of Middle Ear Infection. *Molecules*. 2020;25(9):2239. doi:10.3390/molecules25092239
10. Smirnov NA, Kudryashov SI, Nastulyavichus AA, et al. Antibacterial properties of silicon nanoparticles. *Laser Phys Lett*. 2018;15(10):105602. doi:10.1088/1612-202X/aad853
11. Colino CI, Lanao JM, Gutierrez-Millan C. Recent advances in functionalized nanomaterials for the diagnosis and treatment of bacterial infections. *Mater Sci Eng C*. 2021;121:111843. doi:10.1016/j.msec.2020.111843
12. Gold K, Slay B, Knackstedt M, Gaharwar AK. Antimicrobial Activity of Metal and Metal-Oxide Based Nanoparticles. *Adv Ther*. 2018;1 (3):1700033. doi:10.1002/adtp.201700033
13. Mitjans M, Marics L, Bilbao M, Maddaleno AS, Piñero JJ, Vinardell MP. Size Matters? A Comprehensive In Vitro Study of the Impact of Particle Size on the Toxicity of ZnO. *Nanomaterials*. 2023;13(11):1800. doi:10.3390/nano13111800
14. Matusoiu F, Negrea A, Nemes NS, et al. Antimicrobial Perspectives of Active SiO2FexOy/ZnO Composites. *Pharmaceutics*. 2022;14(10):2063. doi:10.3390/pharmaceutics14102063
15. Ding Y, Yang IS, Li Z, et al. Nanoporous $TiO_2$ spheres with tailored textural properties: controllable synthesis, formation mechanism, and photochemical applications. *Pro Mater Sci*. 2020;109:100620. doi:10.1016/j.pmatsci.2019.100620
16. Amri F, Septiani NLW, Rezki M, et al. Mesoporous $TiO_2$-based architectures as promising sensing materials towards next-generation biosensing applications. *J Mater Chem B*. 2021;9(5):1189–1207. doi:10.1039/D0TB02292F
17. Querebillo CJ. A Review on Nano Ti-Based Oxides for Dark and Photocatalysis: from Photoinduced Processes to Bioimplant Applications. *Nanomaterials*. 2023;13(6):982. doi:10.3390/nano13060982
18. Wang J, Wang Z, Wang W, et al. Synthesis, modification and application of titanium dioxide nanoparticles: a review. *Nanoscale*. 2022;14 (18):6709–6734. doi:10.1039/D1NR08349J
19. Hou J, Zhao H, Zhang Z, Yu L, Yan X. The antifouling tris-(8-hydroxyquinoline) aluminum: titanium dioxide coatings under visible light. *Surf Coat Technol*. 2023;468:129743. doi:10.1016/j.surfcoat.2023.129743
20. Park S, Keum Y, Park J. Ti-Based porous materials for reactive oxygen species-mediated photocatalytic reactions. *Chem Commun*. 2022;58 (5):607–618. doi:10.1039/D1CC04858A
21. Schutte-Smith M, Erasmus E, Mogale R, Marogoa N, Jayiya A, Visser HG. Using visible light to activate antiviral and antimicrobial properties of $TiO_2$ nanoparticles in paints and coatings: focus on new developments for frequent-touch surfaces in hospitals. *J Coat Technol Res*. 2023;20 (3):789–817. doi:10.1007/s11998-022-00733-8
22. Ghorashi MS, Madaah Hosseini HR, Mohajerani E, Pedroni M, Taheri Ghahrizjani R. Enhanced $TiO_2$ Broadband Photocatalytic Activity Based on Very Small Upconversion Nanosystems. *J Phys Chem C*. 2021;125(25):13788–13801. doi:10.1021/acs.jpcc.1c01403

23. Žerjav G, Teržan J, Djinović P, et al. $TiO_2$-β-$Bi_2O_3$ junction as a leverage for the visible-light activity of $TiO_2$ based catalyst used for environmental applications. *Catal. Today*. 2021;361:165–175. doi:10.1016/j.cattod.2020.03.053
24. Shin J, Naskar A, Ko D, Kim S, sun KK. Bioconjugated Thymol-Zinc Oxide Nanocomposite as a Selective and Biocompatible Antibacterial Agent against *Staphylococcus* Species. *Int J Mol Sci*. 2022;23(12):6770. doi:10.3390/ijms23126770
25. Dai S, Jiang L, Liu L, et al. Photofunctionalized and Drug-Loaded $TiO_2$ Nanotubes with Improved Vascular Biocompatibility as a Potential Material for Polymer-Free Drug-Eluting Stents. *ACS Biomater Sci Eng*. 2020;6(4):2038–2049. doi:10.1021/acsbiomaterials.0c00041
26. Luo Y, Song Y. Mechanism of Antimicrobial Peptides: antimicrobial, Anti-Inflammatory and Antibiofilm Activities. *Int J Mol Sci*. 2021;22 (21):11401. doi:10.3390/ijms222111401
27. Huang X, Li G. Antimicrobial Peptides and Cell-Penetrating Peptides: non-Antibiotic Membrane-Targeting Strategies Against Bacterial Infections. *Infect Drug Resistance*. 2023;16:1203–1219. doi:10.2147/IDR.S396566
28. Ganesan N, Mishra B, Felix L, Mylonakis E. Antimicrobial Peptides and Small Molecules Targeting the Cell Membrane of Staphylococcus aureus. *Microbiol Mol Biol Rev*. 2023;87(2):e00037–22. doi:10.1128/mmbr.00037-22
29. Amiss AS, Henriques ST, Lawrence N. Antimicrobial peptides provide wider coverage for targeting drug-resistant bacterial pathogens. *Pept Sci*. 2022;114(2):e24246. doi:10.1002/pep2.24246
30. Bai X, Li L, Liu H, Tan L, Liu T, Meng X. Solvothermal Synthesis of ZnO Nanoparticles and Anti-Infection Application in Vivo. *ACS Appl Mater Interfaces*. 2015;7(2):1308–1317. doi:10.1021/am507532p
31. González-Campo A, Orchard KL, Sato N, Shaffer MSP, Williams CK. One-pot, in situ synthesis of ZnO-carbon nanotube–epoxy resin hybrid nanocomposites. *Chem Commun*. 2009;1(27):4034. doi:10.1039/b905353k
32. Hou Z, Lu J, Fang C, et al. Underlying Mechanism of In vivo and In vitro Activity of C-terminal–amidated Thanatin Against Clinical Isolates of Extended-Spectrum β-lactamase–Producing Escherichia coli. *J Infect Dis*. 2011;203(2):273–282. doi:10.1093/infdis/jiq029
33. Sabirov A, Metzger DW. Mouse models for the study of mucosal vaccination against otitis media. *Vaccine*. 2008;26(12):1501–1524. doi:10.1016/j.vaccine.2008.01.029
34. Mittal R, Sanchez-Luege SV, Wagner SM, Yan D, Liu XZ. Recent Perspectives on Gene-Microbe Interactions Determining Predisposition to Otitis Media. *Front Genetics*. 2019;10. doi:10.3389/fgene.2019.01230
35. Kono M, Umar NK, Takeda S, et al. Novel Antimicrobial Treatment Strategy Based on Drug Delivery Systems for Acute Otitis Media. *Front Pharmacol*. 2021:12. doi:10.3389/fphar.2021.640514
36. Kasza K, Gurnani P, Hardie KR, Cámara M, Alexander C. Challenges and solutions in polymer drug delivery for bacterial biofilm treatment: a tissue-by-tissue account. *Adv. Drug Delivery Rev.* 2021;178:113973. doi:10.1016/j.addr.2021.113973
37. Khan I, Saeed K, Khan I. Nanoparticles: properties, applications and toxicities. *Arabian J Chem*. 2019;12(7):908–931. doi:10.1016/j.arabjc.2017.05.011
38. Ruddaraju LK, Pammi SVN, Guntuku GS, Padavala VS, Kolapalli VRM. A review on anti-bacterials to combat resistance: from ancient era of plants and metals to present and future perspectives of green nano technological combinations. *Asian J. Pharm. Sci.* 2020;15(1):42–59. doi:10.1016/j.ajps.2019.03.002
39. Chen Q, Zhu W, Ni Y, Yuan H. The Properties of the $CH_3NH_3PbI_3/TiO_2$ Composite Layer Prepared from PbO-$TiO_2$ Mesoporous Layer under Air Ambience. *Coatings*. 2023;13(4):669. doi:10.3390/coatings13040669
40. Smijs TG, Pavel S. Titanium dioxide and zinc oxide nanoparticles in sunscreens: focus on their safety and effectiveness. *NSA*. 2011;4:95–112. doi:10.2147/NSA.S19419
41. Pant B, Ojha GP, Kuk YS, Kwon OH, Park YW, Park M. Synthesis and Characterization of ZnO-$TiO_2$/Carbon Fiber Composite with Enhanced Photocatalytic Properties. *Nanomaterials*. 2020;10(10):1960. doi:10.3390/nano10101960
42. Zhou T, Wang J, Chen S, et al. Bird-nest structured ZnO/$TiO_2$ as a direct Z-scheme photoanode with enhanced light harvesting and carriers kinetics for highly efficient and stable photoelectrochemical water splitting. *Appl Catal B*. 2020;267:118599. doi:10.1016/j.apcatb.2020.118599
43. Najibi Ilkhechi N, Mozammel M, Yari Khosroushahi A. Antifungal effects of ZnO, $TiO_2$ and ZnO-$TiO_2$ nanostructures on Aspergillus flavus. *Pesticide Biochemistry Physiol*. 2021;176:104869. doi:10.1016/j.pestbp.2021.104869
44. Wang P, Jiang S, Li Y, et al. Virus-like mesoporous silica-coated plasmonic Ag nanocube with strong bacteria adhesion for diabetic wound ulcer healing. *Nanomed Nanotechnol Biol Med*. 2021;34:102381. doi:10.1016/j.nano.2021.102381
45. Park SW, Lee D, Choi YS, et al. Mesoporous $TiO_2$ implants for loading high dosage of antibacterial agent. *Appl. Surf. Sci.* 2014;303:140–146. doi:10.1016/j.apsusc.2014.02.111
46. Yang L, Kuang H, Liu Y, et al. Mechanism of enhanced antibacterial activity of ultra-fine ZnO in phosphate buffer solution with various organic acids. *Environ Pollut*. 2016;218:863–869. doi:10.1016/j.envpol.2016.08.015
47. Shi LE, Li ZH, Zheng W, Zhao YF, Jin YF, Tang ZX. Synthesis, antibacterial activity, antibacterial mechanism and food applications of ZnO nanoparticles: a review. *Food Additives and Contaminants: Part A*. 2014;31(2):173–186. doi:10.1080/19440049.2013.865147
48. Hou Y, Feng J, Wang Y, Li L. Enhanced antibacterial activity of Ag-doped ZnO/polyaniline nanocomposites. *J Mater Sci Mater Electron*. 2016;27 (7):6615–6622. doi:10.1007/s10854-016-4669-0
49. Gudkov SV, Burmistrov DE, Serov DA, Rebezov MB, Semenova AA, Lisitsyn AB. A Mini Review of Antibacterial Properties of ZnO Nanoparticles. *Front Phys*. 2021;9. doi:10.3389/fphy.2021.641481
50. Sá AS, De lima IS, Honório LM, et al. ROS-mediated antibacterial response of ZnO and ZnO containing cerium under light. *Chem Pap*. 2022;76 (11):7051–7060. doi:10.1007/s11696-022-02390-y
51. Nicolas P. Multifunctional host defense peptides: intracellular-targeting antimicrobial peptides. *FEBS J*. 2009;276(22):6483–6496. doi:10.1111/j.1742-4658.2009.07359.x
52. Huang Y, Huang J, Chen Y. Alpha-helical cationic antimicrobial peptides: relationships of structure and function. *Protein and Cell*. 2010;1 (2):143–152. doi:10.1007/s13238-010-0004-3
53. He B, Ma S, Peng G, He D. TAT-modified self-assembled cationic peptide nanoparticles as an efficient antibacterial agent. *Nanomed Nanotechnol Biol Med*. 2018;14(2):365–372. doi:10.1016/j.nano.2017.11.002
54. Xuan J, Feng W, Wang J, et al. Antimicrobial peptides for combating drug-resistant bacterial infections. *Drug Resist Updates*. 2023;68:100954. doi:10.1016/j.drup.2023.100954

55. Peschel A, Sahl HG. The co-evolution of host cationic antimicrobial peptides and microbial resistance. *Nat Rev Microbiol*. 2006;4(7):529–536. doi:10.1038/nrmicro1441
56. Li X, Liu W, Sun L, et al. Effects of physicochemical properties of nanomaterials on their toxicity. *J Biomed Mater Res Part A*. 2015;103(7):2499–2507. doi:10.1002/jbm.a.35384
57. Kim KM, Song JH, Kim MK, et al. Physicochemical analysis methods for nanomaterials considering their toxicological evaluations. *Mol Cell Toxicol*. 2014;10(4):347–360. doi:10.1007/s13273-014-0039-2
58. Wang X, Cui X, Zhao Y, Chen C. Nano-bio interactions: the implication of size-dependent biological effects of nanomaterials. *Sci China-Life Sci*. 2020;63(8):1168–1182. doi:10.1007/s11427-020-1725-0